Comparison of ultrafine-grain isotropic graphite prepared from microcrystalline graphite and pitch coke

Zhao He [a,b,c], Jinliang Song [d], Zheng Wang [a,b], Xiaohui Guo [a], Zhanjun Liu [a, b *], T. James Marrow [c]

[a] Key Laboratory of Carbon Materials, Institute of Coal Chemistry, Chinese Academy of Sciences, Taiyuan 030001, China

[b] Center of Materials Science and Optoelectronics Engineering, University of Chinese Academy of Sciences, Beijing 100049, China

[c] Department of Materials, University of Oxford, Oxford OX1 3PH, UK

[d] Shanghai Institute of Applied Physics, Chinese Academy of Sciences, Shanghai 201800, China

Abstract

As a metamorphic product of coal, microcrystalline graphite is of ultrafine polycrystalline structure with near-isotropic and highly graphitized characteristics, which endows itself with great potential as filler for ultrafine-grain isotropic graphite (UGIG). In this work, two kinds of microcrystalline graphite based UGIG, MGG12 and MGG8, are prepared by a liquid mixing process from microcrystalline graphite filler with an average particle size of 12 and 8 μm, respectively. For comparison, pitch coke based UGIG, PCG8, is prepared as control sample from pitch coke filler with an average particle size of 8 μm using the same pitch binder and preparation method. Compared with PCG8, MGG12 and MGG8 exhibit many structure and property advantages such as higher density, higher graphitization degree, higher thermal conductivity, higher isotropy, lower coefficient of thermal expansion, smaller median pore diameter, lower porosity and better barrier property to molten fluoride salt. Notably, due to the smallest median pore diameter (0.431 μm) of MGG8 among these three kinds of UGIG, the

* Corresponding author
E-mail address: zjliu03@sxicc.ac.cn (Zhanjun Liu)

molten salt weight gain ratio of MGG8 is only 0.13 wt% under 5 atm, which is much lower than 16.1 wt% and 15.1 wt% for PCG8 and MGG12 under 4 atm, respectively. These advantages indicate that microcrystalline graphite may have advantages over pitch coke as filler for the preparation of UGIG for molten salt applications such as molten salt reactor. In addition, the relevant mechanisms are analyzed and discussed by comparison of the structural characteristics of microcrystalline graphite and pitch coke.

Keywords: Ultrafine-grain isotropic graphite, Microcrystalline graphite, Pitch coke, Pitch binder, Molten salt barrier property

1. Introduction

Molten salts are widely used in advanced technologies such as molten salt reactor (MSR) [1], solar thermal power plant [2, 3] and high temperature thermal energy storage system [4]. However, molten salts are often highly corrosive to the structural materials used in these environments, which discourages the application of molten salt technologies and increases the technical cost. Graphite materials have outstanding comprehensive property including high chemical stability, high temperature mechanical strength, high thermal conductivity as well as excellent nuclear properties, and thus are suitable for working with molten salts. Notably, the pore size of graphite materials for molten salt applications must be small enough to keep molten salts from penetrating. For example, the pore size of nuclear graphite for MSR must be less than 1 μm to prevent molten fluoride salt from penetrating into it and affecting its service performance [5-7]. However, large pores are inevitable in synthetic graphite materials for the following two main reasons. On the one hand, the pores are mainly caused by the decomposition and volatilization of pitch binder during baking process. On the other hand, connatural pores and mutually imperfect filling effects of raw materials can also form pores in

synthetic graphite materials. So far, graphite materials that satisfy this criterion are hard to obtain, and it is urgent to develop graphite materials that satisfy the pore size requirements of molten salt applications to promote the development of this advanced technology.

Previous researches have indicated that the self-sintered method [8, 9], the precursor impregnation pyrolysis method [10, 11] and the use of ultrafine filler [12-14] are promising methods to obtain graphite materials with small pore size. Unfortunately, self-sintered graphite derived from mesocarbon microbead or green coke is easy to crack due to its large volumetric shrinkage during the sintering process, which severely limits its application potential. Moreover, the precursor impregnation pyrolysis method is likely to lead to the inhomogeneity of impregnation and worsen the structure homogeneity of graphite material. Although ultrafine filler is often used to prepare ultrafine-grain isotropic graphite (UGIG), it is still challenging to prepare large-sized products due to several technical problems. Firstly, it is difficult to prevent agglomeration when ultrafine filler mixed with pitch binder. Secondly, the low thermal conductivity of ultrafine petroleum/pitch coke (the most common filler) formed green body increases the risk of cracking due to the large temperature gradient between surface and center of green body during the calcination procedure. Additionally, due to the release of large amounts of volatile components (more pitch binder is usually used in the kneading process of ultrafine filler) that cause a large volume change and the reduction of escape channels for volatile components, the ultrafine filler formed green body tends to crack during the calcination procedure. Both raw material and preparation technique are two key factors that determine the structure and properties of graphite materials. Therefore, selection of suitable raw material and optimization of preparation technique are keys to the development of large-sized UGIG for molten salt applications.

As a metamorphic product of coal, microcrystalline graphite has great potential as filler for UGIG

due to its unique structural characteristics [15, 16]. On the one hand, microcrystalline graphite is composed of randomly oriented graphitic micro-crystallites, which is conducive to facilitating the wetting of pitch binder and ensuring the isotropic property of final graphite block. On the other hand, the high thermal conductivity and the highly graphitized structure are beneficial for facilitating the green body baking process and improving the graphitization degree of the final graphite block, respectively. In addition, the continuous emergence and development of advanced technologies such as high-temperature purification can effectively remove impurities dispersed in microcrystalline graphite ores, which makes it easier to obtain cost-effective and high-purity microcrystalline graphite for the preparation of UGIG [15]. Previous researches have indicated that graphitic fillers such as natural flake graphite [13, 14], microcrystalline graphite [15, 16] and recycled nuclear graphite [17, 18] can be used to produce isotropic graphite. Although microcrystalline graphite is abundant in China, it is not as widely used as natural flake graphite. At present, microcrystalline graphite is mainly used in low-end fields such as pencil lead and carburant for steelmaking. Recently, microcrystalline graphite is adopted to develop numerous products such as anode materials [19, 20], electromagnetic absorbers [21], graphene nanosheets [22-27] and refractories [28, 29]. However, it is difficult to achieve large-scale application of microcrystalline graphite in the short term because of some technical barriers to break through. Therefore, it is important and meaningful to develop value-added materials from microcrystalline graphite. And development of UGIG from filler of microcrystalline graphite will certainly promote and accelerate the rise of China's microcrystalline graphite industry. In terms of the agglomeration of ultrafine filler in the kneading process, the liquid mixing process may be an effective solution [12, 14, 30-32]. Compared with conventional mixing process, liquid mixing process, in which ultrafine-grain filler is mixed with the solution of pitch and tetrahydrofuran, has advantages in

preventing filler from being conglomerated and improving the coalescent ability as well as homogeneity of raw materials, and thus is conducive to improving the microstructure and properties of obtained graphite. Moreover, liquid mixing process is also conducive to decreasing of the pitch binder dosage, which can decrease the difficulties of carbonization and strengthen the ability to produce UGIG with large dimensions. Based on the above analysis, it is meaningful and feasible to prepare UGIG from filler of ultrafine microcrystalline graphite by a liquid mixing process for molten salt applications such as MSR.

In this work, microcrystalline graphite and pitch coke are used as filler to prepare three kinds of UGIG by a liquid mixing process. Microstructures and properties of these three kinds of UGIG are investigated and compared with each other. Especially, the molten fluoride salt and mercury infiltration behaviors in these three kinds of UGIG are evaluated to compare their differences in barrier property related to molten salt applications such as MSR. It is found that microcrystalline graphite gives rise to UGIG with smaller pore size and therefore better molten salt barrier property than pitch coke filler under the same experiment process. In addition, the property differences of these three kinds of UGIG are elucidated based on the differences in filler type and average particle size.

2. Experimental

2.1. Materials

Microcrystalline graphite with 99.9 wt% carbon, which was purified by a high temperature purification process, was provided by Hunan Chenzhou Lutang Microcrystalline Graphite Carbon Co. LTD, Hunan Province, China. Both pitch coke and coal-tar pitch were provided by Jining Keneng New Carbon Materials Technology Co. Ltd., Shangdong Province, China. The microcrystalline graphite was pulverized into two powders with an average particle size of 12 and 8 μm. The pitch coke was

pulverized into a powder with an average particle size of 8 μm for comparative analysis. As shown in Fig. 1, the morphology and microstructure of pitch coke and microcrystalline graphite (both of which have an average particle size of 8 μm) are quite different. There are obvious graphitic micro-crystallites in the microcrystalline graphite, but not in the pitch coke. UGIG were prepared using microcrystalline graphite and pitch coke as filler and coal-tar pitch as binder and impregnating agent. Tetrahydrofuran, which was selected as a solvent to dissolve coal-tar pitch, was provided by Sinopharm Group Chemical Reagent Beijing Co. Ltd., Beijing City, China. FLiNaK salt (46.5% LiF-11.5% NaF-42% KF, mole ratio), one potential coolant for MSR [1], was used as impregnation salt.

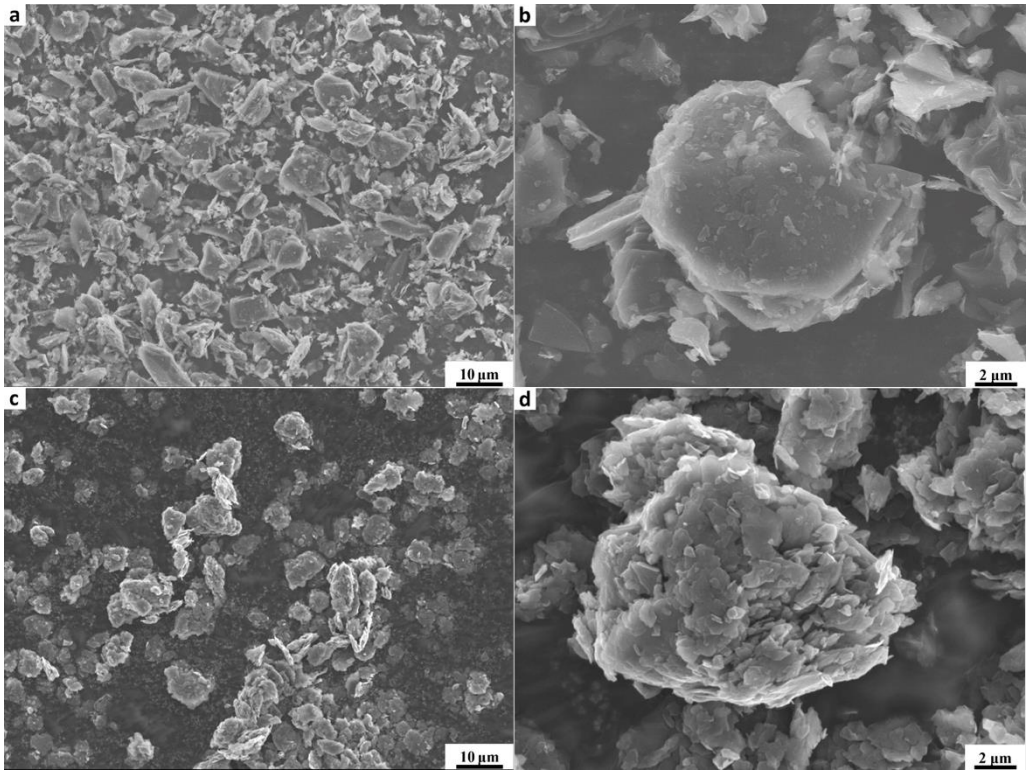

Fig. 1 Morphology images of pitch coke (a, b) and microcrystalline graphite (c, d).

2.2. Sample preparation

Different amounts of coal-tar pitch binder were selected according to the average particle size of filler. Specifically, filler with an average particle size of 8 μm (both microcrystalline graphite and pitch coke) was kneaded with 40 wt% coal-tar pitch binder, and 35 wt% coal-tar pitch binder was kneaded

with microcrystalline graphite with an average particle size of 12 μm. The specific mixing process is shown in Fig. 2 and mainly consisted of the following steps: coal-tar pitch binder was firstly dissolved in the tetrahydrofuran organic solvent at 60 °C, with a solvent dosage of no less than 80 wt%; These three kinds of filler (both microcrystalline graphite and pitch coke) and dissolved pitch were kneaded at 60 °C for 1 hour; The obtained slurry was put in a blast drying oven and dried at about 100 °C for 4 hours to remove the solvent; The mixed materials in the dry state were pulverized into fine powders after being cooled to room temperature. The fine powders were then pressed into cylindrical green bodies by isostatic pressing at 200 MPa. The obtained green bodies were calcined at 1000 °C for 3 hours. Following this, one pitch impregnation process was conducted on these carbonized bodies for increasing their densities. The final graphite blocks were obtained after the secondary calcination and subsequent graphitization processes, which was done at a graphitization temperature of 2500 °C. The as-prepared graphite blocks were labelled as microcrystalline graphite-based graphite (MGG8 and MGG12) and pitch coke-based graphite (PCG8), and number 8 and 12 referred to the average particle size of filler (microcrystalline graphite and pitch coke). To interpret the experimental results, coal-tar pitch and pitch coke were subjected to the same carbonization and graphitization treatments along with the graphite blocks preparation process.

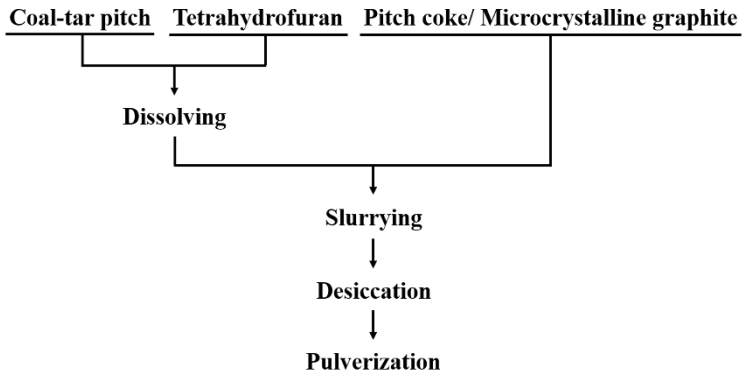

Fig. 2 The technical flow of the liquid mixing process.

2.3. Sample characterization methods

The elemental compositions of pitch and pitch coke were analyzed by an elemental analyzer (Elementar VARIO EL cube). The softening point of pitch was measured by ring and ball method. The carbon yield of pitch was tested in accordance with Conradson method. The ash content of pitch was tested according to ASTM D2415-1966. The ash content of pitch coke was tested according to ASTM D4422-19. A helium pycnometer (Micromeritics, Accupyc 1330) was adopted to test the density of filler, and the Archimedes method was used to evaluate the sample apparent density. X-ray diffraction (XRD, Bruker D8 Advance, λ=0.15406 nm) and Raman spectroscopy (HORIBA Jobin-Yvon, LabRam HR800, λ=514 nm) were adopted to characterize the crystal phase structure of sample. A field emission scanning electron microscope (SEM, JSM-7001F) was used to characterize the microstructure morphology. A laser flash technique (Nano Flash Apparatus, LFA 447/2-2, NETZSCH) and a differential scanning calorimeter (DSC, 200F3, NETZSCH) were adopted to measure the thermal diffusivity and the specific heat of sample, respectively. Equation (1), $k = a \times C_p \times \rho$ (1), was adopted to calculate the thermal conductivity (k) of sample. And the a, C_p and ρ in equation (1) refer to thermal diffusivity, specific heat and density, respectively. A dilatometer (Netzsch DIL 402 PC, NETZSCH) was used for the coefficient of thermal expansion (CTE) of sample, and the anisotropic factor (φ) was calculated according to equation (2): $\varphi = \alpha_{\perp}/\alpha_{||}$ (2), where $\alpha_{\perp}$ and $\alpha_{||}$ refer to the CTE perpendicular and parallel to the molding pressure, respectively. An automatic mercury porosimeter (AutoPore IV 9500) was adopted to quantify the pore structural information. The flexural strength was obtained by three-point bending method and the compressive strength was tested according to ASTM C695-91 [33]. The average values of each structural and performance parameters were obtained from test results of five samples.

The molten salt infiltration experiments were carried out to evaluate and compare the molten salt barrier properties of the as-prepared three kinds of UGIG. The specific experiment process has been reported by previous works [10, 11]. The molten salt infiltration experiments were conducted at 650 °C to ensure the completely melting of FLiNaK salt (melting point of 454 °C). The infiltration time under a series of infiltration pressures (1, 1.5, 2, 2.5, 3, 4 and 5 atm) was set at 12 hours. Equation (3), $\eta = (m_2\text{-}m_1)/m_1$ (3), was adopted to calculate the weight gain ratio (η, wt%) for each graphite sample (namely its infiltration amount of molten FLiNaK salt). And the m_1 and m_2 in the equation (3) refer to the weight values of every graphite sample before and after the molten salt treatment, respectively.

3. Results and discussion

3.1. *Microstructures and thermo-physical properties of UGIG*

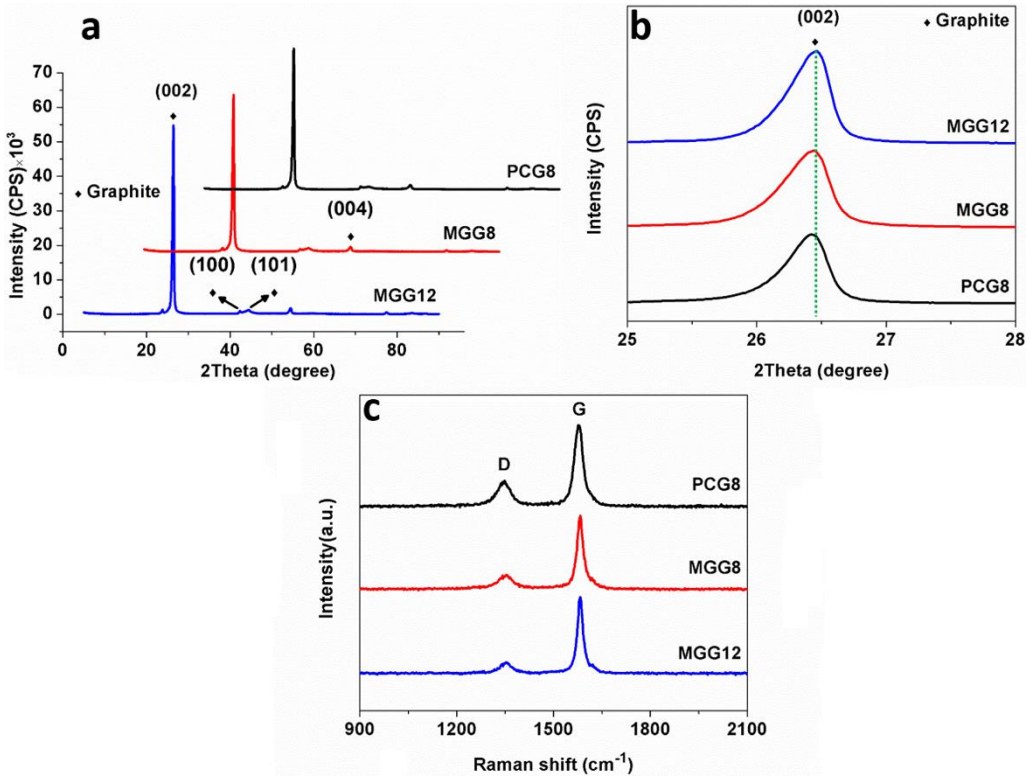

Fig. 3 XRD spectra (a, b) and Raman spectra (c) of UGIG.

As shown in Fig. 3a-b, these three kinds of UGIG have typical graphitic structure. Compared with PCG8, the diffraction peaks of MGG8 and MGG12 are slightly narrower and the (002) peak also tends

to a larger 2Theta (Fig.3a-b). The interlayer spacing d_{002} can be calculated out according to the Bragg diffraction: $d_{002} = \frac{\lambda}{2sin\theta}$ (4). L_a, the mean dimension of crystallite parallel to the diffracting plane (002), can be calculated out by using the Scherrer equation: $L_a = \frac{9.5}{d_{002}-3.354}$ (5). The graphitization degree (g) can be calculated out according to the following equation: $g = \frac{0.3440-d_{002}}{0.3440-0.3354}$ (6). The mean d_{002} for MGG8 and MGG12 are 0.33681 nm and 0.33655 nm, respectively, and both of which are smaller than the 0.33707 nm of PCG8. The mean dimensions of crystallite L_a for MGG8 and MGG12 are 67.0 nm and 81.3 nm, respectively, and both of which are larger than 56.9 nm of PCG8. The graphitization degrees of MGG8 and MGG12 are as high as 83.5% and 86.4%, respectively, whereas PCG8 only has a graphitization degree of 80.6%. Typical peaks of D band and G band of UGIG were tested and shown in Fig. 3c. As shown in Fig. 3c, the D band and G band of the Raman spectra of UGIG were at about 1350 cm^{-1} and 1580 cm^{-1}, respectively. And these two bands represent the first-order defect-induced Raman features and the doubly degenerate phonon mode with E_{2g} symmetry for a sp^2 carbon network, respectively. The more obvious D band in the Raman spectra of PCG8 indicates it has more defects than MGG8 and MGG12. The intensity ratio of D band and G band (I_D/I_G) can also be adopted to evaluate the graphitization degree of UGIG [34]. The I_D/I_G indicates that MGG8 (0.25) and MGG12 (0.20) have higher graphitization degree than PCG8 (0.34), which is consistent with the results of XRD. As these three kinds of UGIG are prepared by the same preparation process, their differences in crystal structural parameter can be ascribed to the effect of filler. The graphitization degree of microcrystalline graphite ores (from Lutang of Chenzhou) has reported to be as high as 88.8% [15], not to mention its high-temperature purification products. Therefore, the intrinsic higher crystallinity of the microcrystalline graphite filler than graphitized pitch coke, may cause the higher graphitization degree of MGG8 and MGG12 than PCG8. The higher

graphitization degree of MGG12 than MGG8 may be ascribed to the effects of different filler size and coal-tar pitch binder dosage. Firstly, finer average particle size of the microcrystalline graphite filler contains more defects and may introduce more defects in the final graphite product, which is confirmed by Fig. S1a-b, Table S3 and Table 1. Secondly, with the increase of coal-tar pitch binder dosage, there may be a lower crystallization of the final graphite products due to the higher crystallinity of filler particles than the binder after graphitization (Fig. S1a-b and Table S3) [35-37]. The graphitization degrees of MGG12 and MGG8 are comparable to that of commercial nuclear graphite such as 84.8% of IG-110 and 83.5% of NBG-18 [38], and much higher than 74% of NPIG [8]. The graphitization degree of nuclear graphite is vital to its irradiation property including irradiation lifetime. Specifically, the higher the graphitization degree, the slower the damage accumulation rate, which prolongs the irradiation lifetime [15]. These results show that UGIG with a high degree of graphitization can be obtained at a low graphitization temperature (for example, the 2500 °C used in this experiment) by using microcrystalline graphite filler.

Table 1 Properties of UGIG.

Properties	PCG8	MGG12	MGG8
Grain size (μm)	8.00±0.23	12.00±0.18	8.00±0.24
Apparent density (g/cm^3)	1.80±0.02	1.84±0.01	1.87±0.01
Compressive strength (MPa)	93.6±1.8	80.5±2.0	89.4±1.6
Flexure strength (MPa)	44.8±1.2	38.8±1.5	42.1±1.3
L_a (nm)	56.9±0.3	81.3±0.2	67.0±0.3
Graphitization degree (%)	80.6±0.2	86.4±0.2	83.5±0.2
Anisotropic factor ($\alpha_{\perp}/\alpha_{||}$)	1.09±0.02	1.06±0.01	1.04±0.01

Thermal conductivity (298 K, W/m·K)	106.4±1.5	126.5±1.3	116.3±1.4
CTE (298-573 K, 10^{-6}/K)	5.1±0.1	4.6±0.1	4.8±0.1
Median pore diameter (volume, μm)	1.601±0.028	1.310±0.035	0.431±0.032
Open porosity (%)	16.2±0.2	15.6±0.3	13.8±0.2
Total porosity (%)	20.4±1.2	18.6±0.6	17.3±0.6

214 Note: The total porosity was calculated based on the theory density of graphite (2.26 g/cm^3).

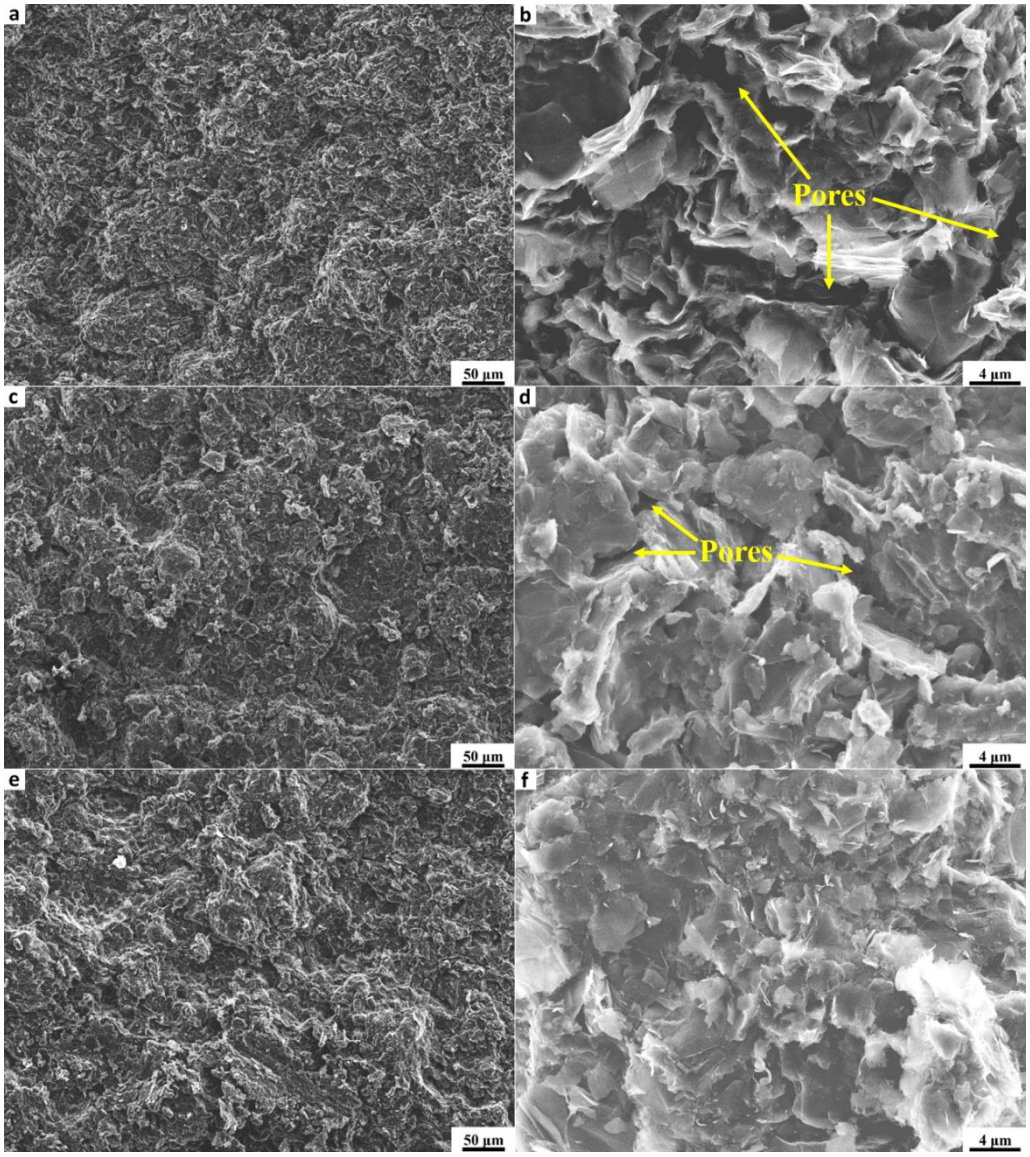

215

216 Fig. 4 SEM images of PCG8 (a, b), MGG12 (c, d) and MGG8 (e, f).

217 SEM images of these three UGIG are presented in Fig. 4. These images show that MGG12 and

MGG8 are more compact than PCG8. Specifically, as labeled by yellow arrows in Fig. 4b, some large pores exist in PCG8. Compared with PCG8, the pores in MGG12 are smaller in size (Fig. 4d), and in MGG8, there are only some quite small pores observed (Fig. 4f).

As shown in Table 1, although these three kinds of UGIG were prepared by the same preparation process, there are significant differences in their structures and properties. MGG12 and MGG8 are superior to PCG8 in terms of structural compactness and other properties except mechanical properties, for which MGG8 is still comparable to PCG8. The density differences between UGIG prepared from filler of microcrystalline graphite and pitch coke can be interpreted as follows. Firstly, the higher true density of microcrystalline graphite (2.2 g/cm^3) than pitch coke (1.95 g/cm^3) endows a higher density to MGG8 and MGG12 than PCG8. Secondly, microcrystalline graphite is more easily wetted by coal-tar pitch binder than pitch coke [16], which is conducive to the penetration of coal-tar pitch binder into the pores of microcrystalline graphite particles, the improvement of interfacial strength, the reduction of pore formation as well as the increase of final graphite density. Thirdly, the low surface friction of microcrystalline graphite is conducive to reducing the forming resistance and further improve the density of green body and subsequent graphitization product [15]. In addition, the graphitic micro-crystallites in microcrystalline graphite may facilitate the graphitization process of the coal-tar pitch binder carbon coated around them, which is also conducive to the increase of the density of final graphite. These factors can not only increase the density of graphite block prepared from microcrystalline graphite filler, but also reduce the pore size and porosity of graphite block. Within a certain range, the smaller the size of filler is, the easier it is to achieve the compact accumulation during the forming process, resulting in higher density, smaller pore size and lower porosity of MGG8 than MGG12. The highest density and graphitization degree, the largest mean dimensions of crystallite L_a,

the smallest pore size and lowest porosity of MGG12 endow it with the highest thermal conductivity among these three kinds of UGIG. There are randomly oriented graphitic micro-crystallites in microcrystalline graphite, but not in pitch coke. This structural difference gives the MGG12 and MGG8 better isotropic properties than PCG8, as shown by the anisotropic factors of MGG12 (1.06) and MGG8 (1.04), which are lower than PCG8 (1.09). The finer the average particle size of the microcrystalline graphite filler is, the more spherical the filler particle is, and the easier it is to realize random orientation during the forming process. Therefore, MGG8 has lower anisotropic factor than MGG12. The low anisotropic factor (1.04) of MGG8 is conducive to ensuring its structural integrity and even service life in the MSR irradiation environment. Although MGG12 and MGG8 have higher density, smaller pore size and lower porosity than PCG8, their CTEs are lower than PCG8. This should be ascribed to their higher graphitization degree than PCG8. Similarly, the lower graphitization degree of PCG8 may be partly responsible for its higher mechanical strength than MGG12 and MGG8. Furthermore, microcrystalline graphite is one kind of highly graphitized filler, which is stable and almost no structural changes occurring during the graphitization process. However, pitch coke is amorphous, which can convert into graphitic structure along with coal tar pitch binder carbon during the graphitization process. And strong chemical bonds are formed during this transformation process, which is also conducive to improving the mechanical strength of PCG8.

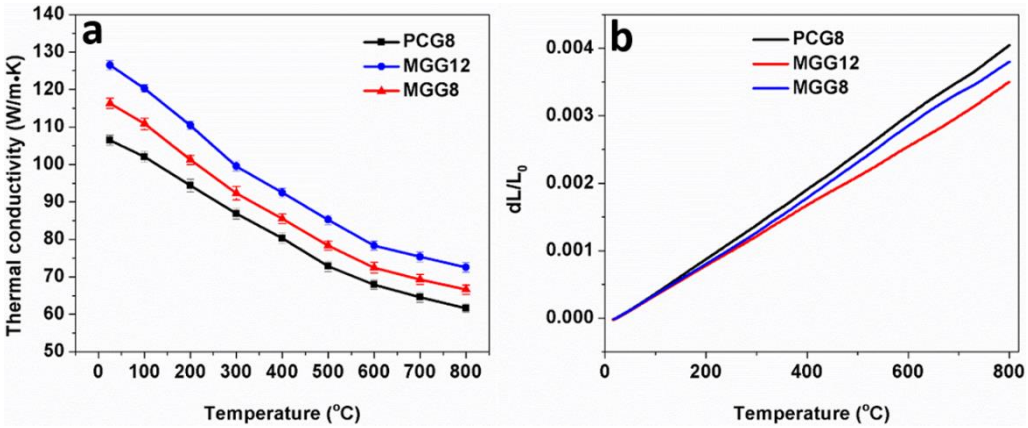

Fig. 5 Thermal conductivity (a) and representative thermal expansion (b) curves of UGIG.

For graphite materials used in molten salt environment, especially nuclear graphite in MSR, both good thermal conductivity and low CTE are key properties, which are conducive to facilitating thermo transfer of system, reducing thermal stress and enhancing structural integrity of graphite components [34]. Fig. 5a shows the variation of the thermal conductivities of these three kinds of UGIG with temperature. The thermal conductivities of all UGIG decrease with the increase of test temperature owing to the decrease of phonon motion mean free path and the increase of phonon scattering intensity at elevated temperature [39]. Specifically, the thermal conductivity of PCG8 decreases from 106.4 W/m·K at 25 °C to 61.6 W/m·K at 800 °C. Similarly, the thermal conductivities of MGG12 and MGG8 decrease from 126.5 W/m·K and 116.3 W/m·K at 25 °C to 72.5 W/m·K and 66.7 W/m·K at 800 °C, respectively. Higher thermal conductivities of MGG12 and MGG8 than that of PCG8 can be ascribed to the effect of filler type. The grain size of MGG8 is 8 μm, which is less than half grain size of commercial nuclear graphite IG-110 (20 μm) prepared from petroleum coke filler, however, the thermal conductivity of MGG8 is comparable to that of IG-110 (116 W/m·K at 25 °C) [10, 11, 13] and much higher than that of NPIG (46 W/m·K at 25 °C) [8]. The thermal conductivities of MGG12 and MGG8 may be further improved by increasing the graphitization temperature from the 2500 °C used in this study. These results indicate that microcrystalline graphite has advantage over petroleum/pitch coke as filler for the preparation of UGIG with high thermal conductivity. Fig. 5b shows the thermal expansion behaviors of these three kinds of UGIG. For PCG8, the CTE between 25 °C to 300 °C is 5.1×10^{-6}/K, which is much higher than 4.6×10^{-6}/K of MGG12 and 4.8×10^{-6}/K of MGG8. As MGG12 and MGG8 are much more compact than PCG8, their higher graphitization degree may be the key reason for their lower CTEs. Moreover, the CTEs between 25 °C to 300 °C of MGG8 and MGG12 are

much lower than that of UGG-2 (5.3×10^{-6}/K) [12] and NPIG (6.0×10^{-6}/K) [8], which indicates that microcrystalline graphite may have advantages on preparation of UGIG with low CTE.

3.2. *Mercury and molten salt infiltration into UGIG*

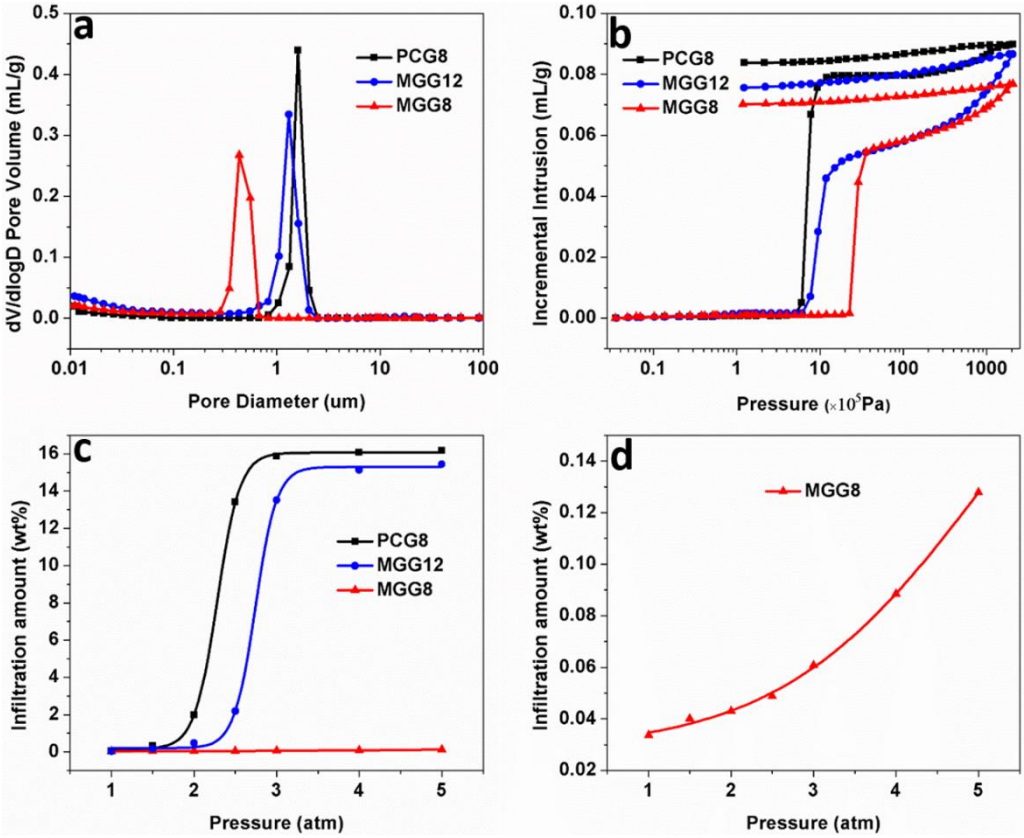

Fig. 6 (a) pore diameter distribution, (b) mercury injection amount with the increase of pressure and (c, d) salt weight gain ratio of UGIG.

Fig. 6a-b show the pore size distributions and mercury infiltration curves of these three kinds of UGIG. Although prepared by the same preparation process, they are still quite different in compactness. Specifically, the density of PCG8 is 1.80 g/cm^3, which is lower than 1.84 g/cm^3 of MGG12 and 1.87 g/cm^3 of MGG8. Moreover, the median pore diameter and porosity of PCG8 (1.60 μm and 16.2%) are larger and higher than that of MGG12 (1.31 μm and 15.6%) and MGG8 (0.43 μm and 13.8%). MGG12 and MGG8 are much more compact than PCG8, which indicates that microcrystalline graphite may have advantages over pitch coke as filler for the preparation of UGIG with high compactness. Previous

293 works have confirmed that the pore size of nuclear graphite for MSR must be less than 1 μm to prevent
294 molten fluoride salt from penetrating into it [5-7], so molten fluoride salt is expected to penetrate both
295 PCG8 and MGG12 easily via their large pores (>1 μm). The salt weight gain ratios are presented in
296 Fig. 6c-d. And it is difficult for molten salt to penetrate into PCG8 and MGG12 under low infiltration
297 pressure. Nevertheless, as the infiltration pressure increased to 2.5 atm and 3 atm, the amounts of
298 molten salt that penetrated into PCG8 and MGG12 increased to 13.4 wt% and 13.5 wt%, respectively.
299 And as the infiltration pressure increased to above 4 atm, their molten salt infiltration amounts
300 saturated at about 16.1 wt% and 15.1 wt%, respectively. In comparison, MGG8 exhibits much better
301 molten salt barrier property than PCG8 and MGG12. Even as the infiltration pressure increased to 5
302 atm, MGG8 resisted the penetration of molten salt effectively with the infiltration amount of 0.13 wt%,
303 which is well below 0.45 wt% for UUG-2 under the same experimental condition [12] and 0.5 wt%
304 (the specified value for MSR under a specified pressure of 5 atm) [5]. The mercury infiltration curves
305 are presented in Fig. 6b and show three stages. In the first stage ($<5.03\times10^5$ Pa), mercury is difficult
306 to penetrate into PCG8. Once the test pressure exceeds 5.03×10^5 Pa, mercury can penetrate into PCG8
307 easily and rapidly until the test pressure increasing to 9.40×10^5 Pa (the end of second stage). The
308 starting pressure of this second stage is defined as the threshold pressure. When the test pressure
309 exceeds 9.40×10^5 Pa (the third stage), some mercury can fill the newly accessible voids caused by the
310 destruction of brittle closed pores [40]. Both MGG12 and MGG8, show the same stages, but mercury
311 cannot fill into them significantly until higher threshold pressures (6.10×10^5 Pa and 22.50×10^5 Pa,
312 respectively). Compared with PCG8, the smaller median pore diameter of MGG12 (1.310 μm) and
313 MGG8 (0.431 μm) causes a higher capillary force, thus a higher test pressure is required to make
314 mercury penetrate into MGG12 and MGG8 rapidly and significantly. The total mercury penetration

amount of PCG8 is 0.0897 ml/g, which is more than MGG12 (0.0866 ml/g) and MGG8 (0.0768 ml/g), showing there is a higher open porosity of PCG8 compared with that of MGG12 and MGG8. Notably, the average filler size of MGG8 (8 μm) is much larger than that of UGG-2 (5 μm) [12], however, the median pore diameter of MGG8 (0.431 μm) is much samller than that of UGG-2 (0.52 μm) [12], which indicates that microcrystalline graphite may have advantages on preparation of UGIG with small pores.

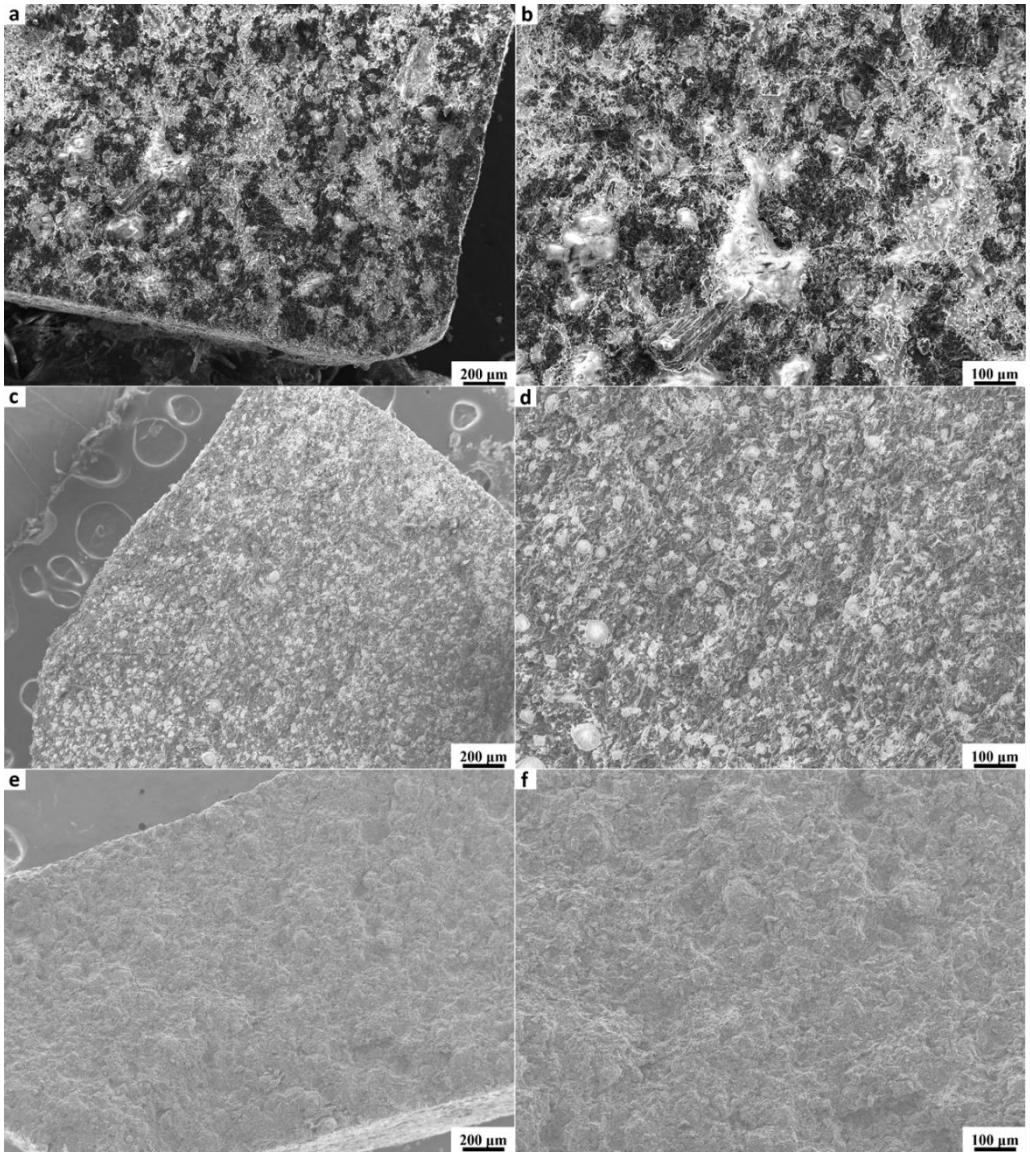

Fig. 7 SEM images of PCG8 at 3 atm (a, b), MGG12 at 3 atm (c, d) and MGG8 at 5 atm (e, f) after molten salt experiments.

Fig. 7 shows the fracture surface images of infiltrated graphite samples. The molten salt volume

proportion (ν, vol%) of each graphite sample can be calculated from its molten salt weight gain ratio (η, wt%) by referring to the next equation: $\nu = \frac{\rho_G}{\rho_{Salt}}\eta$ (7), where ρ_G and ρ_{Salt} are graphite density (see Table 1) as well as molten salt density (2.05 g/cm^3), respectively. For PCG8, when the infiltration pressure is 3 atm, the molten salt volume proportion is as high as 13.93 vol%, which accounts for 86.0% of its open pores (its open porosity is approximately 16.2%). Similarly, the molten salt volume proportion of MGG12 at 3 atm is 12.14 vol%, which accounts for 77.8% of its open pores (its open porosity is approximately 15.6%). This is consistent with Fig. 7a-d, which shows that most pores of PCG8 and MGG12 are filled with white salt particles. For MGG8, even as the infiltration pressure increased to 5 atm, few salt particles can be observed (Fig. 7e-f), which shows that MGG8 can inhibit the penetration of molten salt effectively.

Both mercury and molten FLiNaK salt cannot wet graphite well, so their infiltration behaviors into graphite are comparable [41]. The threshold pressures in FLiNaK salt may be deduced using the Washburn equation [42, 43] for the capillary force $\Delta P = -\frac{4\gamma\cos\theta}{\delta}$ (8), where ΔP, γ, θ and δ refer to the capillary force, surface tension, contact angle and pore size, respectively. A scaling factor (X), for the threshold pressure in salt, for same graphite sample can be defined as $X = \frac{\Delta P_{Hg}}{\Delta P_{Salt}} = \frac{\gamma_{Hg}\cos(\theta_{\mathrm{Hg}})}{\gamma_{Salt}\cos(\theta_{Salt})}$ (9) [44]. For graphite and mercury system, γ_{Hg} and θ_{Hg} are about 485 dyne/cm and 130º, respectively [43]. For graphite and molten FLiNaK salt system, γ_{Salt} and θ_{Salt} are about 160 dyne/cm and 140º, respectively [12], hence the scaling factor X is ~2.54 and the obtained threshold pressures are summarized in Table 2. The calculated threshold pressure of molten FLiNaK salt for MGG8 is 8.86×10^5 Pa (8.74 atm), which is much higher than the specified infiltration pressure for MSR (5 atm) [5].

Table 2 Threshold pressures for UGIG.

Threshold pressure (Pa)	PCG8	MGG12	MGG8
Mercury ($\times 10^5$)	5.03±0.12	6.10±0.15	22.50±0.21
Molten FLiNaK ($\times 10^5$)	1.98±0.05	2.40±0.06	8.86±0.08

To our knowledge, the as-prepared MGG8 derived from microcrystalline graphite filler with an average particle size of 8 μm has never been reported before. Its excellent molten salt barrier property makes it probably be used in molten salt applications including MSR, though if it were considered for use in MSR, irradiation experiments would be indispensable.

4. Conclusion

Based on the design concept of densification of structure, we have experimentally demonstrated a liquid mixing process to prepare UGIG from ultrafine filler of microcrystalline graphite. In addition, the advantages of microcrystalline graphite over pitch coke as filler for UGIG have also been demonstrated. The structure and the excellent properties of MGG8 are derived from the compact accumulation of ultrafine filler, the characteristics of microcrystalline graphite and the advantages of liquid mixing process in mixing ultrafine filler and coal tar pitch binder. The as-prepared MGG8 has high density, high mechanical strength, high graphitization degree, high isotropic property, high thermal conductivity, low CTE, small median pore diameter as well as low porosity. Benefiting from its small median pore diameter, MGG8 exhibits excellent molten salt barrier property and can inhibit the penetration of molten salt effectively. The protocol proposed in this work has shed light on producing high-performance graphite blocks from microcrystalline graphite to satisfy the growing demand for molten salt applications such as MSR, which may facilitate the development of microcrystalline graphite industry.

CRediT authorship contribution statement

Zhao He: Investigation, Formal analysis, Data curation, Writing - original draft, Writing review & editing, Validation, Methodology. **Jinliang Song**: Investigation, Formal analysis. **Zheng Wang**: Formal analysis. **Xiaohui Guo**: Formal analysis. **Zhanjun Liu**: Conceptualization, Funding acquisition, Supervision, Validation, Visualization, Writing - review & editing. **T. James Marrow**: Writing - review & editing.

Declaration of competing interest

The authors firmly declare that they have no competing financial interests or personal relationships that could have appeared to influence the work reported in this paper.

Acknowledgments

Great thanks to the National Natural Science Foundation of China (91860116) for its financial support for this work. This manuscript is written whilst Zhao He is an Academic Visitor at University of Oxford with the financial support of China Scholarship Council (File No. 201904910864).

References

[1] Frandsen BA, Nickerson SD, Clark AD, Solano A, Baral R, Williams J, et al. The structure of molten FLiNaK, J Nucl Mater 2020;537.

[2] Bauer T, Pfleger N, Laing D, Steinmann W-D, Eck M, Kaesche S. High-Temperature Molten Salts for Solar Power Application, in: F.L. Groult (Ed.) Molten Salts Chemistry, Elsevier, Oxford, 2013, p. 415-38.

[3] Shen X, Ding J, Peng Q, Yang J. Application of High Temperature Molten Salt to Solar Thermal Power, Guangdong Chem Ind 2007;34(11):49-52.

[4] Zhong Y, Zhao B, Lin J, Zhang F, Wang H, Zhu Z, et al. Encapsulation of high-temperature inorganic phase change materials using graphite as heat transfer enhancer, Renew Energ 2019;133:240-7.

[5] Briggs RB, Kasten PR. Molten-salt reactor program semiannual progress report. USA: Oak Ridge National Laboratory, ORNL-3419. 1963:71-3.

[6] Mccoy H, Beatty R, Cook W, Gehlbach R, Kennedy C, Koger J, et al. New developments in materials for molten salt reactors. Nucl Appl Technol 1970;8(2):156-69.

[7] M.W. Rosenthal, P.N. Haubenreich, Briggs RB. The Development Status of Molten-Salt Breeder Reactors. USA: Oak Ridge National Laboratory, ORNL-4812. 1972:175-93,273-90.

[8] Song JL, Zhao YL, Zhang JP, He XJ, Zhang BL, Lian PF, et al. Preparation of binderless nanopore-isotropic graphite for inhibiting the liquid fluoride salt and Xe^{135} penetration for molten salt nuclear reactor. Carbon 2014;79:36-45.

[9] Zhao H, He Z, Liu Z, Song J, Tsang DKL, Zhang H. Self-sintered nanopore-isotropic graphite derived from green pitch coke for application in molten salt nuclear reactor. Ann Nucl Energy 2019;131:412-6.

[10] He Z, Lian P, Song Y, Liu Z, Song J, Zhang J, et al. Improving molten fluoride salt and Xe^{135} barrier property of nuclear graphite by phenolic resin impregnation process. J Nucl Mater 2018;499:79-87.
[11] He Z, Lian P, Song Y, Liu Z, Song J, Zhang J, et al. Protecting nuclear graphite from liquid fluoride salt and oxidation by SiC coating derived from polycarbosilane. J Eur Ceram Soc 2018;38(2):453-62.
[12] Lian P, Song J, Liu Z, Zhang J, Zhao Y, Gao Y, et al. Preparation of ultrafine-grain graphite by liquid dispersion technique for inhibiting the liquid fluoride salt infiltration. Carbon 2016;102:208-15.
[13] He Z, Lian P, Song J, Zhang D, Liu Z, Guo Q. Microstructure and properties of fine-grained isotropic graphite based on mixed fillers for application in molten salt breeder reactor. J Nucl Mater 2018;511:318-27.
[14] He Z, Liu Z, Song J, Lian P, Guo Q. Fine-grained graphite with super molten salt barrier property produced from filler of natural graphite flake by a liquid-phase mixing process. Carbon 2019;145:367-77.
[15] Shen K, Huang Z-H, Hu K, Shen W, Yu S, Yang J, et al. Advantages of natural microcrystalline graphite filler over petroleum coke in isotropic graphite preparation. Carbon 2015;90:197-206.
[16] Li K, Shen K, Huang Z-H, Shen W, Yang G, Yang J, et al. Wettability of natural microcrystalline graphite filler with pitch in isotropic graphite preparation. Fuel 2016;180:743-8.
[17] Burchell TD, Pappano PJ. Recycling irradiated nuclear graphite—A greener path forward. Nucl Eng Des 2012;251:69-77.
[18] Liu J, Wang C, Dong L, Liang T. Study on the Recycling of Nuclear Graphite after Micro-Oxidation. Nucl Eng Technol 2016;48(1):182-8.
[19] Kim K-J, Lee T-S, Kim H-G, Lim S-H, Lee S-M. A hard carbon/microcrystalline graphite/carbon composite with a core-shell structure as novel anode materials for lithium-ion batteries. Electrochimi Acta 2014;135:27-34.
[20] Zhao Y, Yang L, Ma C, Han G. One-Step Fabrication of Fluorine-Doped Graphite Derived from a Low-Grade Microcrystalline Graphite Ore for Potassium-Ion Batteries. Energ Fuel 2020;34(7):8993-9001.
[21] Xie W, Zhu X, Yi S, Kuang J, Cheng H, Tang W, et al. Electromagnetic absorption properties of natural microcrystalline graphite. Mater Des 2016;90:38-46.
[22] Xian H, Peng T, Sun H, Wang J. Preparation, characterization and supercapacitive performance of graphene nanosheets from microcrystalline graphite. J Mater Sci - Mater Electron 2014;26(1):242-9.
[23] Lin SF, Liu FX, Chen GH. Effective production of nano-sized graphene via straight-forward exfoliation of microcrystalline graphite. RSC Adv 2014;4(86):45885-9.
[24] Xian H, Peng T, Sun H, Wang J. Preparation of graphene nanosheets from microcrystalline graphite by low-temperature exfoliated method and their supercapacitive behavior. J Mater Sci 2015;50(11):4025-33.
[25] Wang J, Huang J, Yan R, Wang F, Cheng W, Guo Q, et al. Graphene microsheets from natural microcrystalline graphite minerals: scalable synthesis and unusual energy storage. J Materi Chem A 2015;3(6):3144-50.
[26] Xie W, Zhu X, Xu S, Yi S, Guo Z, Kuang J, et al. Cost-effective fabrication of graphene-like nanosheets from natural microcrystalline graphite minerals by liquid oxidation–reduction method. RSC Adv 2017;7(51):32008-19.
[27] Fang C, Zhang Z, Bing X, Lei Y. Preparation, characterization and electrochemical performance of graphene from microcrystalline graphite. J Mater Sci - Mater Electron 2017;28(24):19174-80.
[28] Wang H, Li Y, Sang S, Jin S, Xu Y, Yang K, et al. Microstructures and mechanical properties of Al_2O_3–C refractories using nickel-loaded ultrafine microcrystalline graphite and silicon additives. Ceram Int 2014;40(10):15783-93.
[29] Wang H, Li Y, Zhu T, Fu Z. Strengthening of Al_2O_3-C slide gate plate refractories with microcrystalline graphite. Ceram Int 2017;43(13):9912-8.
[30] Liu Z, Guo Q, Liu L, Chen J, Li J. Improvements in performance and microstructure of doped graphites as plasma-facing materials by a new process. Fusion Eng Des 2007;82(1):55-9.
[31] Liu Z, Guo Q, Shi J, Zhai G, Liu L. Preparation of doped graphite with high thermal conductivity by a liquid mixing process. Carbon 2007;45(9):1914-6.

[32] Liu Z, Guo Q, Song Y, Shi J, Song J, Liu L. Carbon seal materials with superior mechanical properties and fine-grained structure fabricated by a new process. Mater Lett 2007;61(8-9):1816-9.
[33] ASTM C695-91, Standard Test Method for Compressive Strength of Carbon and Graphite, 2010.
[34] Xu S, Kang F. Carbon and graphite materials in nuclear engineering. Beijing (China): Tsinghua University Press. 2010.
[35] Moormann R, Hinssen H-K, Kühn K. Oxidation behaviour of an HTR fuel element matrix graphite in oxygen compared to a standard nuclear graphite. Nucl Eng Des 2004;227(3):281-4.
[36] Wen KY, Marrow TJ, Marsden BJ. The microstructure of nuclear graphite binders. Carbon 2008;46(1):62-71.
[37] Cho YJ, Lu K. Water vapor oxidation behaviors of nuclear graphite IG-110 for a postulated accident scenario in high temperature gas-cooled reactors. Carbon 2020;164:251-60.
[38] Chi S-H, Kim G-C. Comparison of the oxidation rate and degree of graphitization of selected IG and NBG nuclear graphite grades. J Nucl Mater 2008;381(1-2):9-14.
[39] Chakraborty S, Debnath D, Mallick AR, Gupta RK, Ranjan A, Das PK, et al. Microscopic, mechanical and thermal properties of spark plasma sintered ZrB_2 based composite containing polycarbosilane derived SiC. Int J Refract Met Hard Mater 2015;52:176-82.
[40] Pore size distribution and porosity of solid materials by mercury porosimetry and gas adsorption-Part 1: Mercury porosimetry. GB/T 21650.1-2008/ISO15901-1: 2005.
[41] Zhong Y, Zhang J, Lin J, Xu L, Zhang F, Xu H, et al. Mesocarbon microbead based graphite for spherical fuel element to inhibit the infiltration of liquid fluoride salt in molten salt reactor. J Nucl Mater 2017;490:34-40.
[42] Washburn EW. The Dynamics of Capillary Flow. Phys Rev 1921;17(3):273-83.
[43] Awasthi A, Bhatt YJ, Garg SP. Measurement of contact angle in systems involving liquid metals. Meas Sci Technol 1996;7(5):753-7.
[44] He Z, Gao L, Qi W, Zhang B, Wang X, Song J, et al. Molten FLiNaK salt infiltration into degassed nuclear graphite under inert gas pressure. Carbon 2015;84:511-8.